Acta Chemica Scandinavica A 37 (1983) 293–306

Solutions of Chlorine in Molten Chlorides. 2. Solubility and Diffusivity of Chlorine in Chloroaluminate Melts

O. WÆRNES and T. ØSTVOLD

Institutt for uorganisk kjemi, Norges tekniske høgskole, Universitetet i Trondheim, N-7034 Trondheim-NTH, Norway

The reduction of Cl_2 dissolved in basic as well as acidic $AlCl_3$–NaCl and $AlCl_3$–CsCl melts ($X_{AlCl_3} \lesssim 0.50$) has been investigated. The electrochemical techniques chronopotentiometry, chronoamperometry and voltammetry were employed.

The chronopotentiometric results obtained in $AlCl_3$–NaCl melts in the temperature range 160–450 °C did not obey the Sand equation, probably due to adsorption of chlorine on the electrode and/or a high value of the double layer capacity. The results have been corrected according to a model which implies simultaneous reaction of adsorbed and diffusing species (SAR model). Fair agreement with the chronoamperometric results was then obtained. The chlorine diffusivity in the $AlCl_3$–MCl mixtures is in the order of 10^{-5} cm^2 s^{-1}, and is not markedly different in acidic and basic melts.

In the $AlCl_3$–NaCl melts ($0.496 < X_{AlCl_3} < 0.52$) and in $AlCl_3$–CsCl melts where $X_{AlCl_3} > 0.50$, the reduction of chlorine is found to be irreversible with $\alpha n_a \approx 0.5$, *i.e.* one-electron transfer in the rate determining step. For the basic $AlCl_3$–CsCl mixtures a nearly reversible two-electron charge transfer was found.

The solubility of chlorine gas in molten $AlCl_3$–CsCl ($0.425 < X_{AlCl_3} < 0.52$) has been determined by a manometric technique. This involves keeping the gas volume above the melt constant and to measure the pressure decrease as the gas dissolves in the liquid. The solubility is around 5×10^{-6} mol cm^{-3} and is decreasing with increasing temperature. There is no tendency to a drastic change in the solubility around the melt composition corresponding to $X_{AlCl_3} = 0.50$.

In a recent paper from this laboratory solutions of chlorine in some alkali chloride melts were studied.[1] Solubilities and electrochemical diffusivities were measured. In the present paper analogous data in chloroaluminate melts are reported.

PRINCIPLES

Chlorine solubility measurements. The equilibrium (1) is studied:

$$Cl_2(g) = Cl_2(\text{dissolved}) \qquad (1)$$

Assuming that Henry's law is valid for the solute and that $Cl_2(g)$ obeys the ideal gas law with a standard state of 1 mol cm^{-3} for the dissolved gas and 1 atm for the pure gas, the equilibrium constant is equal to the Henry's law constant.

$$K_H = \frac{c_{Cl_2}(\text{diss})}{P_{Cl_2}(g)} = \frac{\Delta P V_o \rho}{RTw\Delta P_{eq}} \qquad (2)$$

ΔP is the pressure drop due to dissolution of chlorine. V_o is the volume of gas above the melt reduced to the volume this gas would have at the temperature T.[1-3] This temperature was normally 25 °C. ρ is the density of the melt, R the gas constant, w the weight of salt and ΔP_{eq} the change in equilibrium pressure after an addition of chlorine gas to the volume above the melt.

Chronopotentiometric measurements. The fundamental equation for chronopotentiometry (semiinfinite linear diffusion to a plane electrode) is the Sand equation [4]

$$\tau^{1/2} = \frac{\pi^{1/2} nFAcD^{1/2}}{2I} = \frac{\pi^{1/2} nFcD^{1/2}}{2i} \qquad (3)$$

0302-4377/83 $02.50

τ is the transition time, n the number of electrons in the overall electrochemical reaction, F the Faraday constant, A the electrode area, c the concentration of Cl_2 dissolved in the melt, D the chlorine diffusion constant, I the applied current and i the current density (I/A). The product $I\tau^{1/2}$ (or $i\tau^{1/2}$) should be independent of the applied current and the chlorine diffusion constant may be determined.

Corrections for the inconstancy of the chronopotentiometric constant ($I\tau^{1/2}$ in eqn. (3)) at short transition times have been considered by several authors.[5-11] The increase in $I\tau^{1/2}$ with decreasing transition time is most frequently caused by the distribution of the current between two or more simultaneous processes. The electrolysis of the electroactive species diffusing to the electrode may be complicated by the charging of the electrical double layer, formation or reduction of oxide films at the electrode and/or electrolysis of electroactive species adsorbed on the electrode. An approximate method of treating these effects is to consider the total current as the sum of four constant currents giving the equation (4) [8,9]

$$I\tau^{1/2} = \frac{\pi^{1/2}nFAcD^{1/2}}{2} + \frac{(C_l)_{av}\Delta EA}{\tau^{1/2}} + \frac{Q_{ox}A}{\tau^{1/2}} + \frac{nFA\Gamma}{\tau^{1/2}} \quad (4)$$

where $(C_l)_{av}$ is the average double layer capacity in the potential interval ΔE, Q_{ox} is the amount of electricity required for oxide film formation or reduction, and Γ is the amount of electroactive species adsorbed on the electrode. The other symbols have been defined previously. The first term on the right hand side of eqn. (4) is the "true" chronopotentiometric constant, while the additional correction terms are all of the same form. By rearranging this equation we get eqn. (5),

$$I\tau = \frac{nFAc(\pi D\tau)^{1/2}}{2} + B \quad (5)$$

where B is an overall correction factor. The assumption of constant currents for the different processes during electrolysis implies the simultaneous reaction of adsorbed reactant and diffusing species (SAR mechanism). Thus only a single transition time is expected.

If, however, the adsorbed species are completely reduced prior to the reduction of the diffusing species (AR, SR mechanism) [6,11] two transition times corresponding to the two processes should ideally be observed and $I\tau$ should be proportional to I^{-1}.

A third model requires that the adsorbed layer is being reduced at the end of the diffusion controlled reaction (SR, AR mechanism).[6,11] In this case $(I\tau)^{1/2}$ should be proportional to $I^{-1/2}$ and two distinct transition times would ideally be observed.

From eqn. (5) it is seen that a plot of $I\tau$ *versus* $\tau^{1/2}$ should give a straight line with finite intercept. The intercept may then give information on the amount of adsorbed species or some of the other terms in eqn. (4). From the slope of the line the "true" chronopotentiometric constant, $(I\tau^{1/2})_{corr}$, (or directly the diffusion coefficient) may be determined. Distinction between the various reaction mechanisms discussed is usually based on a best fit comparison of experimental data with the model equations.

Potential–time relations for a number of common reduction mechanisms, derived by several authors, have been summarized by Reinmuth.[12] For a reversible electrochemical reduction where the product of electrolysis is insoluble (or soluble with activity 1 at the electrode surface as in this case for the Cl^- ion) eqn. (6) may be derived from the Nernst equation [12,13]

$$E = E^\circ + \frac{RT}{nF}\ln\frac{2I}{nAF\pi^{1/2}D^{1/2}} + \frac{RT}{nF}\ln(\tau^{1/2}-t^{1/2}) \quad (6)$$

and a plot of the quantity $\ln(\tau^{1/2}-t^{1/2})$ *versus* E, where t is the time, should yield a straight line with the slope RT/nF.

The potential of the working electrode for an irreversible electrochemical reduction involving one rate-determining step is given by eqn. (7),[12,14]

$$E = E_o + \frac{RT}{\alpha n_a F}\ln\frac{2k_s}{\pi^{1/2}D^{1/2}} + \frac{RT}{\alpha n_a F}\ln(\tau^{1/2}-t^{1/2}) \quad (7)$$

where n_a is the number of electrons involved in the rate-determining charge transfer step, α is a transfer coefficient and k_s is the heterogeneous rate constant for the forward electrochemical process when $E=0$.

Chronoamperometry. In a chronoamperometric experiment, a potential step is applied to the

working electrode and the resulting current–time response is measured. In the simplest case the initial potential of the working electrode is sufficiently positive that the reduction does not proceed, and the potential attained by the step is sufficiently negative to immediately drive the surface concentration of the reactant to zero. Fick's law of diffusion solved with initial and boundary conditions for this case gives eqn. (8).[4]

$$It^{1/2} = \frac{nFAcD^{1/2}}{\pi^{1/2}} \tag{8}$$

This equation, known as the Cottrell equation, shows that a diffusion controlled electrolysis of a reactant gives a current decaying as a $t^{-1/2}$ function. If the current at any time, t_x, is plotted against the value of the applied potential, a current–potential curve for the reaction results. If the applied potentials correspond to the plateau of such a current–potential curve and the product $It^{1/2}$ is independent of time, the diffusion coefficient can be determined.

A current–potential curve, constructed from current–time curves, may yield information on the reduction mechanism. For a reversible electrochemical reduction where the product of electrolysis is insoluble (or soluble with activity 1 at the electrode surface as in the present case) eqn. (9) may be derived from the Nernst equation,[15]

$$E = E^\circ + \frac{RT}{nF} \ln \frac{(\pi t)^{1/2}}{nAFD^{1/2}} + \frac{RT}{nF} \ln(I_l - I) \tag{9}$$

where I_l is the limiting current corresponding to the plateau of the current–potential curve.

For an irreversible charge transfer reduction the analog equation is [16]

$$E = \text{const.} + \frac{RT}{\alpha n_a F} \ln \frac{I_l - I}{I} \tag{10}$$

The rate constant of the reaction may be determined from current–time curves at short times according to the method suggested by Oldham and Osteryoung.[17]

Voltammetry. Cyclic voltammetry provides several measurable parameters as function of scan rate: the net currents at the peaks of the cathodic and anodic response (I_p), the peak potentials (E_p), the separation between the cathodic and anodic peak (ΔE_p) and the half peak potential ($E_{p/2}$, the potential where $I = \frac{1}{2} I_p$).

For a reversible electrochemical reduction where the product is insoluble (or soluble with activity 1 at the electrode surface) Berzins and Delahay [18] and Mamantov *et al.*[15] derived the eqns. (11)–(13).

$$I_p = \frac{0.610(nF)^{3/2} AcD^{1/2} v^{1/2}}{(RT)^{1/2}} \tag{11}$$

$$E_p = E^\circ + \frac{RT}{nF} \ln \gamma c - 0.8540 \frac{RT}{nF} \tag{12}$$

$$E_p - E_{p/2} = -0.77 \frac{RT}{nF} \tag{13}$$

Corresponding relations for an irreversible electrochemical reduction are [19–21]

$$I_p = \frac{0.500 n(\alpha n_a)^{1/2} F^{3/2} AcD^{1/2} v^{1/2}}{(RT)^{1/2}} \tag{14}$$

$$E_p = E^\circ - \frac{RT}{\alpha n_a F}\left[0.780 + 0.5 \ln\left[\frac{D\alpha n_a F v}{RT}\right] - \ln k_s\right] \tag{15}$$

$$E_p - E_{p/2} = -1.857 \frac{RT}{\alpha n_a F} \tag{16}$$

From eqn. (15) it follows that the peak potential is a function of the potential scan rate, thus

$$(E_p)_2 - (E_p)_1 = 0.5 \frac{RT}{\alpha n_a F} \ln\left(\frac{v_1}{v_2}\right) \tag{17}$$

Subscript 1 and 2 corresponds to the different scan rates v_1 and v_2, respectively. An increase in the scan rate yields a cathodic shift in peak potential.

EXPERIMENTAL

Chemicals. Aluminium chloride from Fluka AG, was purified by distillation in evacuated and sealed quartz glass tubes furnished with quartz glass frits. The temperature was kept just above the melting point. The aluminium chloride vapour was transported through the frit by means of a small temperature gradient along the tube. The distillation was terminated when about 90 % of the material had been transported to the cool part of the tube. This procedure was repeated

three times. The purification of the alkali chlorides are described elsewhere.[1]

Mixtures of aluminium chloride and alkali chlorides (52 mol % $AlCl_3$) were made by melting and subsequent filtering of appropriate amounts of purified $AlCl_3$ and MCl in evacuated and sealed quartz glass tubes. After remelting, the filtrate was properly mixed and quenched to prevent any phase separation. An entire batch was used for one experiment.

All handling of purified salts were performed in an N_2-atmosphere glovebox where the water vapour level was constantly monitored and kept below 2 ppm.

Electrochemical measurements. The equipment and experimental procedure are described by Wærnes [2] and Wærnes *et al.*,[1] and only a few essential details will be given here.

The electrochemical experiments were performed with a potentiostat/galvanostat (Model 551) together with an analog function generator (Model 566) and a multifunction interface (Model 563) from AMEL, Milano, Italy. When operating in galvanostatic mode a puls generator (made in our workshop) was connected to a mercury-wetted relay in Model 551. This generator was introduced to cut the current at a certain time to prevent metal reduction at the working electrode.

A Nicolet Explorer 2090-3A digital storage oscilloscope with plug-in unit 206-1 (Nicolet Instrument Corp., Madison, Wisconsin) was used. This instrument provides numerical display of accurate voltage and time values for any selected waveform point, and the stored data could be recorded if necessary on an external Linseis LY 822 X–Y recorder.

For the $AlCl_3$–NaCl system (max. temp. 230 °C) the electrochemical cell was immersed in a Pyrex beaker (5 litre) containing a well-stirred eutectic KNO_3–$NaNO_2$ bath. The temperature was kept constant to ±0.5 °C by a heater, a stirrer and a Eurotherm PID regulator (Eurotherm Ltd., Sussex, England). The bath temperature was determined by a Pt/Pt10 %Rh thermocouple.

For the $AlCl_3$–CsCl system the cell was placed in a gold-plated transparent quartz glass tube furnace (Trans Temp., Inc., Cambridge, Massachusetts). The temperature profile in the middle zone of the furnace was $<\pm 1$ °C. The temperature was controlled by a Eurotherm PID regulator and was measured with a Pt/Pt10 %Rh thermocouple under the cell close to the outside cell wall. The actual melt temperature was found by calibration, correlating melt temperature and temperature outside the cell.

Using the gold furnace and the nitrate/nitrite bath, visual observation of the melt and electrodes was possible.

In the chloroaluminate melts the plane working electrode, sealed in a pyrex tube, as well as the cylindrical reference and counter electrodes were made of vitreous carbon since graphite showed considerable swelling and disintegration in these melts. To determine the composition in the $AlCl_3$–MCl mixture the following procedure was used: The starting composition was always 52 mol % $AlCl_3$. By adding MCl crystals to the mixture through the top of the cell at relatively high chlorine flowrate back diffusion of air was prevented. Solid MCl could visually be observed on the basic side ($X_{AlCl_3}<0.50$) after equilibration. The melt composition is thus given by the intercept between the liquidus line and the actual temperature.

Solubility measurements. The method used for measuring chlorine solubility is, in principle, the same as the one used by Wærnes *et al.*[1] and Andresen *et al.*[22] Due to high vapour pressures in chloroaluminate melts, however, the difference in chlorine solubility between two chlorine pressures were determined.[2,23] Due to the high vapour pressure the chlorine gas dissolved in these melts was removed by reducing the chlorine pressure to ~300 Torr, allowing the melt to remain at this pressure for equilibration. By again increasing the chlorine pressure to ~1000 Torr, a new solubility experiment could be performed.

RESULTS

Chlorine solubilities. The solubilities of chlorine in fused $AlCl_3$–CsCl mixtures have been determined in order to calculate the diffusion coefficients of chlorine. For comparison with literature data, solubility measurements in NaCl were also performed.[1]

The Henry's law test, based on the differential pressure change method,[2,23] is shown in Fig. 1 for Cl_2 dissolved in $AlCl_3$–CsCl melts. In this test, the upper and the lower pressure drop are plotted *versus* the upper and lower equilibrium pressures.[2,23] When four or more of these pressure drops (from the same experiment) lie on the same straight line through the origin Henry's law is confirmed.

The Henry's law constants, K_H, are determined from eqn. (2), where the recently measured density data [24] for $AlCl_3$–CsCl melts are used. The mean values of K_H with standard deviations are given in Table 1.

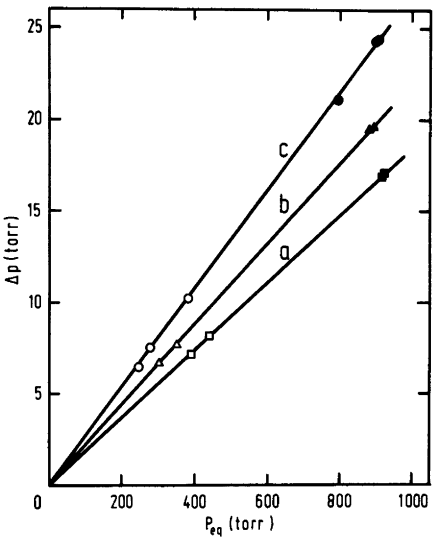

Fig. 1. Test of the validity of Henry's law based on the differential pressure change technique for Cl_2 in $AlCl_3$–CsCl. The filled and open symbols represent upper and lower equilibrium pressures, respectively. *a*–627 °C, X_{AlCl_3}=0.52; *b*–377 °C, X_{AlCl_3}=0.52; *c*–390 °C, X_{AlCl_3}=0.425.

Diffusion coefficients of chlorine.

Chronopotentiometry.

Chronopotentiometric measurements have been performed in $AlCl_3$–NaCl and $AlCl_3$–CsCl melts saturated with chlorine. Representative cathodic chronopotentiometric curves are shown in Fig. 2. The measured transition times, τ, together with the values of $I\tau^{1/2}$ are given by Wærnes.[2]

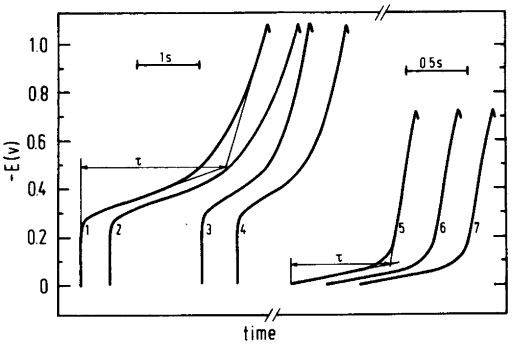

Fig. 2. Chronopotentiometric curves for the reduction of Cl_2 at a plane vitreous carbon electrode. Electrode area, A=0.0535 cm^2. Curves 1–4, acidic $AlCl_3$–NaCl melt at 229 °C, I=0.3, 0.3, 0.4, 0.4 mA. Curves 5–7, basic $AlCl_3$–CsCl melt at 448 °C, I=0.5 mA.

For the $AlCl_3$–CsCl system plots of $\tau^{1/2}$ *versus* inverse current were linear at all temperatures and compositions. As the curves also pass close to the origin eqn. (3) is valid, *i.e.* a single diffusion controlled reaction. The diffusion

Table 1. Solubility of chlorine in molten $AlCl_3$–CsCl mixtures.

Composition	Temp. (°C)	$(K_H \pm SD)10^6$ (mol cm^{-3} atm^{-1})
X_{AlCl_3}=0.52	377	5.22±0.12
	427	4.75
	477	4.21
	527	4.21
	627	3.73±0.01
	727	3.60
X_{AlCl_3}=0.435	360 [a]	5.59±0.29
X_{AlCl_3}=0.425	390 [a]	5.53±0.03

[a] Saturated with CsCl. Melt composition is given as the intercept between the liquidus line [25] and the actual melt temperature.

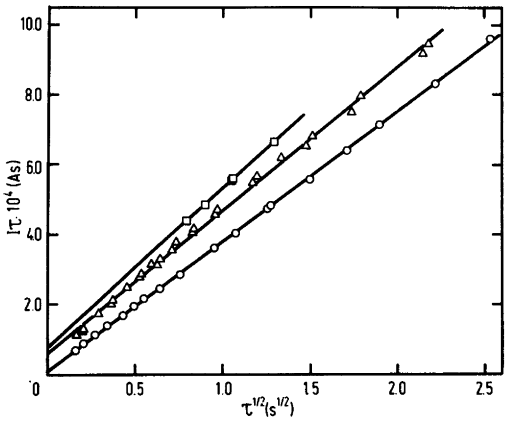

Fig. 3. Test of the SAR mechanism for the reduction of Cl_2 at a plane vitreous carbon electrode in $AlCl_3$–NaCl melts. Electrode area, A=0.0535 cm^2. □ – 157 °C, X_{AlCl_3}=0.51; △ – 187 °C, X_{AlCl_3}=0.51; ○ – 222 °C, X_{AlCl_3}=0.496.

Table 2. Diffusion coefficients of chlorine in molten chloroaluminate melts determined from chronopotentiometric measurements.

System	Temp. (°C)	Chronopot. constant $(i\tau^{1/2}\pm SD)10^3$ ($Acm^{-2}s^{1/2}$)	Number of curves	Diff.coeff. $(D\pm SD)10^5$ ($cm^2\ s^{-1}$)
$AlCl_3$–NaCl	157	8.56±0.07	6	2.22±0.04
X_{AlCl_3}=0.51	177	8.50±0.09	28	3.07±0.07
(Exp. A)	203	8.64±0.06	18	4.72±0.07
	229	8.26±0.04	20	6.16±0.06
X_{AlCl_3}=0.51	162	7.98±0.06	43	2.11±0.03
(Exp. B)	163	8.19±0.06	13	2.26±0.03
	187	7.68±0.06	33	2.94±0.05
	220	7.76±0.04	38	4.82±0.05
X_{AlCl_3}=0.496	163 [a]	7.12±0.04	23	2.01±0.02
(Exp. B)	190 [a]	7.40±0.04	20	3.37±0.04
	222 [a]	6.97±0.02	20	4.71±0.03
$AlCl_3$–CsCl				
X_{AlCl_3}=0.52	390	7.76±0.02	27	7.50±0.04
X_{AlCl_3}=0.435	362 [a]	7.93±0.04	20	7.02±0.07
X_{AlCl_3}=0.425	390 [a]	8.02±0.02	25	8.01±0.04
X_{AlCl_3}=0.40	448 [a]	8.26±0.02	34	10.40±0.05

[a] Saturated with MCl.

coefficients of chlorine are thus determined from the mean values of $i\tau^{1/2}$ at each temperature.

For the $AlCl_3$–NaCl system the product $I\tau^{1/2}$ increased with increasing current. As described previously, this generally indicates adsorption on the electrode or that other complicating processes occur. The experimental data are treated according to eqn. (5) and representative plots are shown in Fig. 3. Each plot gives a straight line with a finite intercept. By linear regression analysis, the "true" chronopotentiometric constant, $(I\tau^{1/2})_{corr}$, was determined from the slope of the curve. The choice of this model will be discussed later. In the following sections the $(i\tau^{1/2})_{corr}$ values for $AlCl_3$–NaCl melts are referred to as $i\tau^{1/2}$.

Calculated values of $i\tau^{1/2}$ along with standard deviations used in subsequent calculations of the diffusion coefficients of chlorine are presented in Table 2. The diffusion coefficients, D, are determined from the Sand equation, eqn. (3), where the concentration, c, is the chlorine solubility (eqns. (20)–(21)). As the overall electrochemical reaction is

$$Cl_2+2e^- \rightarrow 2Cl^- \qquad (18)$$

n in eqn. (3) is equal to 2.

In Table 2 Exp. A and Exp. B refer to different cell fillings. The composition of the acidic $AlCl_3$–NaCl melts ($X_{AlCl_3}>0.5$) given in the table is not exactly 51 mol % $AlCl_3$, and this is discussed later. For $AlCl_3$–NaCl melts saturated with NaCl, the given composition is the average saturation composition within the temperature range.[23] For $AlCl_3$–CsCl melts saturated with CsCl the melt composition is given as the intercept between the liquidus line [25] and the actual melt temperature. For the acidic $AlCl_3$–CsCl mixture negligible change in melt composition was observed, and the diffusion coefficient of Cl_2 is calculated for the initial composition (X_{AlCl_3}=0.52).

Chronoamperometry

Chronoamperometric data from $AlCl_3$–NaCl and $AlCl_3$–CsCl melts are given by Wærnes.[2] A typical current–time curve is shown in Fig. 4.

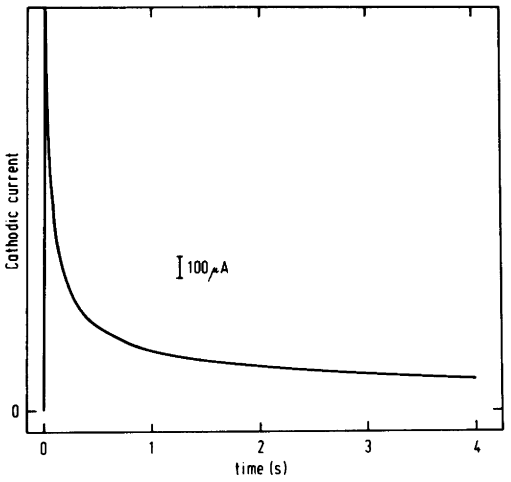

Fig. 4. Chronoamperometric curve for the reduction of Cl_2 at a plane vitreous carbon electrode in a basic $AlCl_3$–CsCl melt at 390 °C. Applied potential was −0.3 V measured against the chlorine reference electrode. Electrode area, A=0.0535 cm^2.

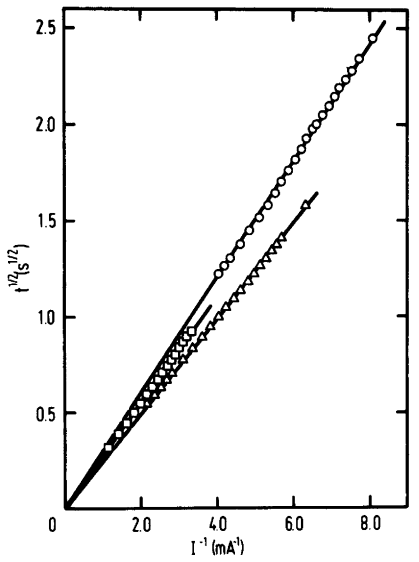

Fig. 5. Tests of the Cottrell equation for the reduction of Cl_2 at a plane vitreous carbon electrode with area A=0.0535 cm^2. ○ – 229 °C, acidic $AlCl_3$–NaCl; □ – 362 °C, basic $AlCl_3$–CsCl; △ – 187 °C, acidic $AlCl_3$–NaCl.

Table 3. Diffusion coefficients of chlorine in molten chloroaluminate melts determined from chronoamperometric measurements.

System	Temp. (°C)	Chronoamp. constant ($it^{1/2}$±SD)10^3 ($Acm^{-2}s^{1/2}$)	Number of curves	Diff.coeff. (D±SD)10^5 (cm^2s^{-1})
$AlCl_3$–NaCl	157	5.84±0.04	4	2.55±0.03
X_{AlCl_3}=0.51	177	5.48±0.07	5	3.15±0.08
(Exp. A)	203	5.62±0.06	11	4.93±0.11
	229	5.61±0.03	2	7.01±0.07
X_{AlCl_3}=0.51	162	5.02±0.03	5	2.06±0.02
(Exp. B)	163	5.49±0.04	7	2.50±0.04
	187	4.66±0.05	9	2.67±0.06
	220	4.68±0.03	7	4.33±0.06
X_{AlCl_3}=0.496				
(Exp. B)	163 [a]	4.73±0.09	12	2.19±0.08
$AlCl_3$–CsCl				
X_{AlCl_3}=0.52	390	5.26±0.01	6	8.50±0.03
X_{AlCl_3}=0.435	362 [a]	5.18±0.02	6	7.39±0.06
X_{AlCl_3}=0.425	390 [a]	5.19±0.02	4	8.28±0.06
X_{AlCl_3}=0.40	448 [a]	5.75±0.07	6	12.43±0.30

[a] Saturated with MCl.

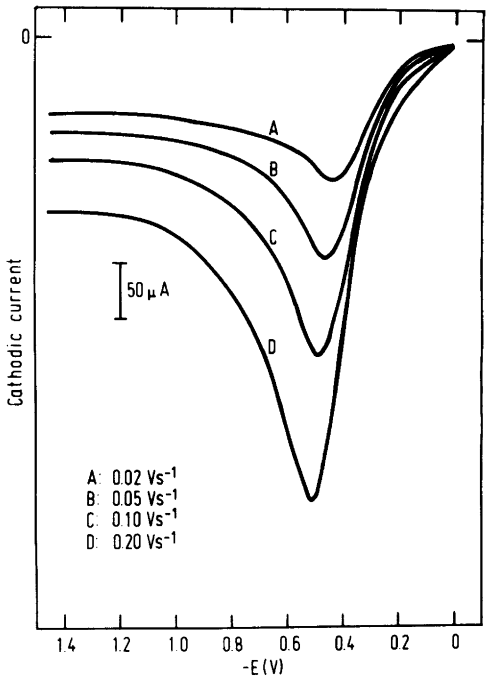

Fig. 6. Voltammograms at a plane vitreous carbon electrode in an acidic $AlCl_3$–NaCl mixture saturated with Cl_2 at 187 °C. Electrode area, A=0.0535 cm^2.

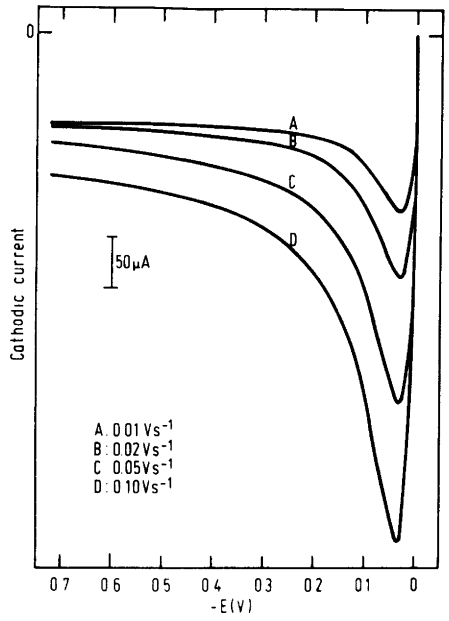

Fig. 7. Voltammograms at a plane vitreous carbon electrode in a basic $AlCl_3$–CsCl melt saturated with Cl_2 at 362 °C. Electrode area, A=0.0535 cm^2.

From each curve more than 15 corresponding I–t values were recorded using the numerical display of the oscilloscope. Fig. 5 shows that plots of $t^{1/2}$ *versus* inverse current were linear and pass close to the origin, thus confirming eqn. (8). The values of the product $it^{1/2}$ given in Table 3 are calculated from the mean values of $It^{1/2}$ obtained from several current–time curves. The diffusion coefficients given in the same table are determined by eqn. (8). The chlorine solubilities, the n value and the melt compositions are the same as those given previously for the chronopotentiometric measurements.

Voltammetry

The diffusion coefficient of chlorine may be determined from voltammetric measurements provided that the reduction mechanism is known. The results obtained in $AlCl_3$–NaCl and $AlCl_3$–CsCl melts using a plane working electrode are given by Wærnes,[2] and are only used in

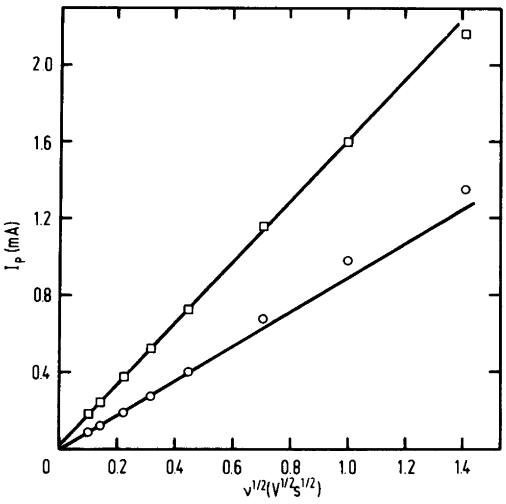

Fig. 8. Peak current *versus* the square root of the scan rate for the reduction of Cl_2 at a plane vitreous carbon electrode with area A=0.0535 cm^2. □ – 448 °C, basic $AlCl_3$–CsCl; ○ – 187 °C, acidic $AlCl_3$–NaCl.

the present paper in the discussion of the reduction mechanism of Cl_2. A series of typical voltammograms are shown in Figs. 6 and 7.

The sweep rate was varied between 0.01 and 2.00 V s^{-1}. The peak current, I_p, tends to show non-linear variation with $v^{1/2}$ at high sweep rates. This was most strongly pronounced for $AlCl_3$–NaCl melts. This is shown in Fig. 8.

DISCUSSION

Experimental accuracy. The relative error in $i\tau^{1/2}$ as expressed by the relation (19)

$$\frac{\Delta(i\tau^{1/2})}{i\tau^{1/2}} = \left[\left(\frac{\Delta I}{I}\right)^2 + \left(\frac{1}{2}\frac{\Delta\tau}{\tau}\right)^2 + \left(\frac{\Delta A}{A}\right)^2\right]^{1/2} \quad (19)$$

where Δ refers to error/uncertainty in the different parameters, is in fair agreement with the standard deviations of the chronopotentiometric constants given in Table 2. A similar equation may be used to estimate the relative error in the diffusion coefficients. The chlorine solubilities are given with a relative accuracy of ~5 % [2,23] and this gives a relative error in D_{Cl_2} of approximately 10–15 %.

The chronopotentiometric constant. Three possible models have been discussed for the correction of $I\tau^{1/2}$ at short transition times. However, the theoretical models are not widely different. There is no *a priori* way of distinguishing between the different mechanisms.

For $AlCl_3$–NaCl melts the increase in $I\tau^{1/2}$ with increasing current was significantly larger than can be attributed to errors arising from incorrect reading of transition times. Plots of the experimental data are well described by a straight line with a finite intercept of the Y-axis for each model. The recorded chronopotentiometric curves show a single transition time. This is expected if the SAR model is valid, while two distinct transition times would ideally be observed for both the AR, SR and SR, AR mechanisms. Since the plot of $I\tau$ *versus* $\tau^{1/2}$ (SAR mechanism) also resulted in intermediate values of the corrected chronopotentiometric constant, this model was preferred to avoid extreme errors.

Further support for the SAR model can be obtained from a comparison between the corrected values of $i\tau^{1/2}$ and the corresponding chronoamperometric constants, $it^{1/2}$. The theoretical value of the ratio $i\tau^{1/2}/it^{1/2}$ is 1.57. An average value of 1.55±0.02 is obtained from the data for the $AlCl_3$–NaCl system given in Tables 2 and 3.

The values of B in eqn. (5) obtained from the SAR model varied in the range 7–70 μA s. The correction decreased with increasing temperature and was highest for melts where $X_{AlCl_3}>0.5$.

Composition of acidic $AlCl_3$–NaCl melts. As previously described, the initial melt composition was 52 mol % $AlCl_3$ in the electrochemical studies. Due to the high vapour pressure of the melt and the flow of chlorine through the electrochemical cell, some $AlCl_3$ was lost during the measurements. Before changing the composition by adding NaCl crystals, melt samples were extracted for chemical analysis. From the amount of NaCl that had to be added to reach the saturation composition ($X_{AlCl_3}=0.496$) it was found that the melt composition had been changed to $0.505<X_{AlCl_3}<0.510$. The analysis of the samples did not, however, give a more accurate melt composition.

Although the solubility of chlorine in $AlCl_3$–NaCl melts changes with composition,[23] the diffusion coefficients seem to be constant in the concentration region $0.496<X_{AlCl_3}<0.52$ (at 160 °C).[2]

Due to the observed changes in the melt composition, all the D values for acidic $AlCl_3$–NaCl melts in Tables 2 and 3 are calculated by using solubility data for an average melt composition of 51 mol % $AlCl_3$. Thus an equation for the temperature dependence of D may be found.

Chlorine solubility. Fig. 9 shows semilogarithmic plots of K_H (mean values) *versus* inverse temperature. For comparison selected literature data [1,22,23] are included. Chlorine solubilities in $AlCl_3$–NaCl melts ($0.45<X_{AlCl_3}<0.6$) are given by eqn. (20).[23,26]

$$\log K_H = -7.927+2.554X_{AlCl_3}+709.7/T \quad (20)$$

(Note an error in eqn. (4) in Ref. 23).

Linear regression analysis of the present experimental data gives eqn. (21).

$AlCl_3$–CsCl($0.425<X_{AlCl_3}<0.52$):

$$\log K_H = -5.824+360.1/T \quad (21)$$

The relative standard deviation in K_H calculated from eqn. (21) is 5 %.

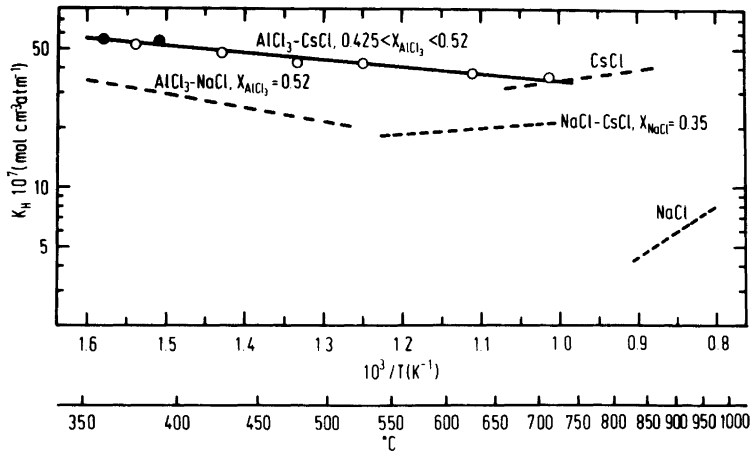

Fig. 9. Semilogarithmic plots of K_H *versus* inverse temperature. The filled symbols correspond to basic $AlCl_3$–CsCl melts where the composition is given by the intercept between the liquidus line [25] and the actual temperature. The dashed lines are results given by Wærnes *et al.*[1] (NaCl, NaCl–CsCl), Andresen *et al.*[22] (CsCl) and Carpio *et al.*[23,26] ($AlCl_3$–NaCl).

The standard enthalpy of dissolution, ΔH°_d, is calculated to be -6.9 ± 0.6 kJ mol^{-1} for chlorine in $AlCl_3$–CsCl melts. This means that the dissolution process is exothermic. Negative values of ΔH°_d are also reported for $AlCl_3$–MCl melts [23,27] and for $0.48<X_{KCl}<0.70$ in the system KCl–$PbCl_2$.[28] In $AlCl_3$–NaCl mixtures where $0.45<X_{AlCl_3}<0.6$, Carpio *et al.*[23] determined ΔH°_d to be -13.6 kJ mol^{-1}. The negative value was explained as due to the successive formation of $AlCl_4^-$, $Al_2Cl_7^-$, $Al_3Cl_{10}^-$ and Al_2Cl_6, which tends to make the melt structure looser and thus less energy is needed to form a void for Cl_2. Increasing polarization energy between Na^+ and Cl_2, and increasing van der Waals interaction forces between Cl_2 and the anions, will also tend to make ΔH°_d more negative when the melt becomes more covalent. This model implies that ΔH°_d decreases with increasing $AlCl_3$-content. Such a decrease was not observed in the relatively narrow composition range investigated by Carpio *et al.*[23] In $AlCl_3$–CsCl melts the polarization energy between Cs^+ and Cl_2 will decrease compared with forces between Na^+ and Cl_2. This will tend to make ΔH°_d less negative in $AlCl_3$–CsCl melts. On the other hand, CsCl may lead to a more "open" structure which results in decreased energy to form a void for Cl_2.

At 500 °C and $X_{AlCl_3}=0.52$ the chlorine solubility in $AlCl_3$–CsCl is twice that in $AlCl_3$–NaCl. The higher solubility in $AlCl_3$–CsCl is expected since the solubilities in pure CsCl are nearly one order of magnitude higher than in pure NaCl.[3,22] Compared with $AlCl_3$–NaCl the "free volume" in the melt may increase due to the larger Cs^+ ion, *i.e.* higher chlorine solubilities in $AlCl_3$–CsCl mixtures.

In molten $AlCl_3$–NaCl, which is assumed not to contain appreciable amounts of Cl_3^-, the chlorine solubility was highest in acidic melts.[23] The present investigation seems to give approximately the same chlorine solubilities in acidic and basic $AlCl_3$–CsCl mixtures (Fig. 9). The spectral changes around the equimolar composition indicates a different solute species as the $AlCl_3$ content is increased above 50 mol %.[24] However, a further discussion will have to be postponed until more spectra and solubility data are available.

Chlorine diffusivity. The temperature dependence of the diffusion coefficients of chlorine is well described by the Arrhenius-type eqn. (22),

$$D = D_o \exp(-E_a^D/RT) \qquad (22)$$

where D_o is a pre-exponential factor, and E_a^D is the activation energy of the diffusion process. Fig. 10 shows semilogarithmic plots of D *versus* inverse temperature. The filled symbols correspond to basic $AlCl_3$–MCl melts ($X_{AlCl_3}<0.5$),

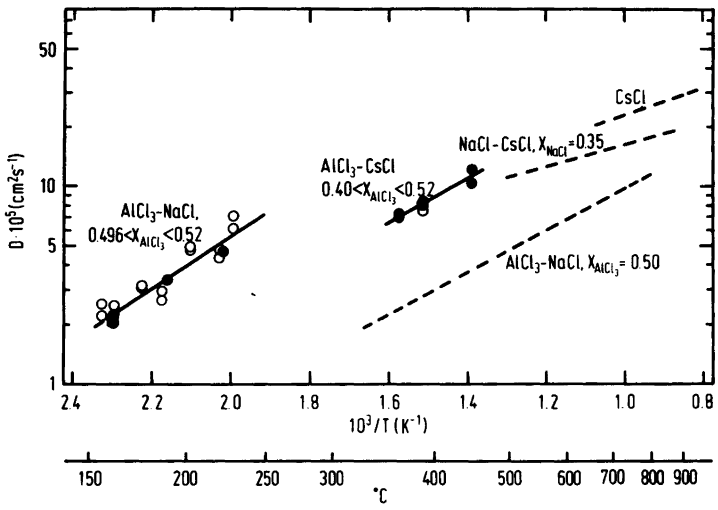

Fig. 10. Semilogarithmic plots of the diffusion coefficient of dissolved Cl_2 as function of inverse temperature. The filled symbols correspond to basic $AlCl_3$–MCl mixtures saturated with MCl. The dashed lines are results given by Wærnes *et al.*[1] (CsCl, NaCl–CsCl) and Mukliev *et al.*[29] ($AlCl_3$–NaCl).

and no drastic change in the diffusion coefficients is observed around the equimolar composition. For comparison selected literature data [1,29] are included.

Linear regression analysis of the data given in Tables 2 and 3 gives the eqns. (23)–(24).

$AlCl_3$–NaCl($0.496<X_{AlCl_3}<0.52$):

$$\log D = -1.593-1328/T \quad (23)$$

$AlCl_3$–CsCl($0.40<X_{AlCl_3}<0.52$):

$$\log D = -2.444-1087/T \quad (24)$$

The relative standard deviation in D calculated by eqns. (23)–(24) is 12 and 7 %, respectively. The activation energy of diffusion, E_a^D, is 25.4±2.0 kJ mol^{-1} for the $AlCl_3$–NaCl mixtures and 20.8±3.1 kJ mol^{-1} for $AlCl_3$–CsCl melts.

From Fig. 10 it is seen that the D values, reported by Mukliev *et al.*,[29] are significantly lower than the present results for $AlCl_3$–MCl melts. Mulkliev *et al.*[29] employed the technique of the weight loss of a platinum rotating disc, and do not report the chlorine solubility used in the calculations. A direct comparison is therefore difficult to perform.

Vetyukov *et al.*[30] have determined the diffusion coefficient of chlorine in basic $AlCl_3$–NaCl melts (790–880 °C) from impedance measurements. In the concentration range $0 \leq X_{AlCl_3} < 0.24$ the diffusion coefficient of chlorine varied one order of magnitude, decreasing to 5×10^{-5} cm^2 s^{-1} (820 °C) with increasing $AlCl_3$ content. In spite of the large differences in temperature and melt composition compared with the present measurements, the values reported by Vetyukov *et al.*[30] seem to be significantly lower than the present results for $AlCl_3$–MCl melts.

Taking into account the lower temperatures, the results for $AlCl_3$–MCl mixtures are not widely different from those found for alkali chlorides (Fig. 10). Moreover, no variation in D is observed close to the equimolar composition in spite of the large variation in the Cl^- activity.[31]

The absorption spectra of $AlCl_3$–NaCl melts ($0.45<X_{AlCl_3}<0.6$) saturated with chlorine did not change dramatically for compositions around $X_{AlCl_3}=0.50$.[23] A pronounced absorption peak at 30 200 cm^{-1}, close to that of gaseous chlorine, is observed. Together with solubility results, this points to Cl_2 as the dissolved species.[23] In $AlCl_3$–CsCl mixtures several spectral changes are observed around the melt composition corresponding to $X_{AlCl_3}=0.50$, probably due to formation of Cl_3^- on the basic side.[24] The absorbance of chlorine increases by a factor of 7 for a

basic melt relative to an acidic melt, while the ratio in molar absorptivity for $AlCl_3$–NaCl is 2 or less.[23]

The high values of the diffusion coefficient of chlorine dissolved in molten alkali chlorides have often been explained by a chain conduction mechanism.[1] This mechanism can not, however, explain the anomalously high diffusion coefficients ($D \geq 10^{-4}$ cm^2 s^{-1}) of other gaseous species like HCl in eutectic LiCl–KCl [32] and O_2 and H_2 in eutectic $NaNO_3$–KNO_3 melts.[33,34]

The results obtained for $AlCl_3$–MCl mixtures can not be explained either by the chain conduction mechanism, as these melts probably do not contain appreciable amounts of Cl_3^- on the acidic side ($X_{AlCl_3} > 0.50$). The relatively high values of D may be due to the "open" structure of these melts caused by the large anion and that diffusion of molecular chlorine therefore is facilitated.

Reduction mechanism of dissolved chlorine. A discussion of the mechanism for the overall reaction

$$Cl_2 + 2e^- \rightarrow 2Cl^-$$

will be given, although a detailed investigation has not been the main objective in the present study. The potentials are measured against a chlorine reference electrode, and the equilibrium potential of the vitreous carbon working electrode did not exceed ±1–3 mV. Equilibrium conditions were reestablished within one minute after each experimental run.

Fig. 6 shows representative voltammetric curves recorded in $AlCl_3$–NaCl melts saturated with chlorine. It is seen that the peak potential, E_p, varies with the scan rate, which is typical for an irreversible process. At each temperature αn_a is calculated by eqn. (17). The value of αn_a appears to be independent of temperature and melt composition, and an average value of 0.63±0.02 is obtained. According to eqn. (16) the peak to half peak separation gives a value of αn_a equal to 0.51±0.02.

From the ratio of voltametric $i_p v^{-1/2}$ to both the chronopotentiometric $i\tau^{1/2}$ and the chronoamperometric $it^{1/2}$, an average value of 0.54±0.02 is calculated for αn_a in the same melts.

As described previously, current–potential curves may be constructed from chronoamperometric curves recorded at different applied potentials. Fig. 11 shows such a curve where the current values are measured at t=2s. A well-defined plateau with a limiting current is obtained for the diffusion process. In the same figure a semilogarithmic plot of $(I_l - I)/I$ *versus* E

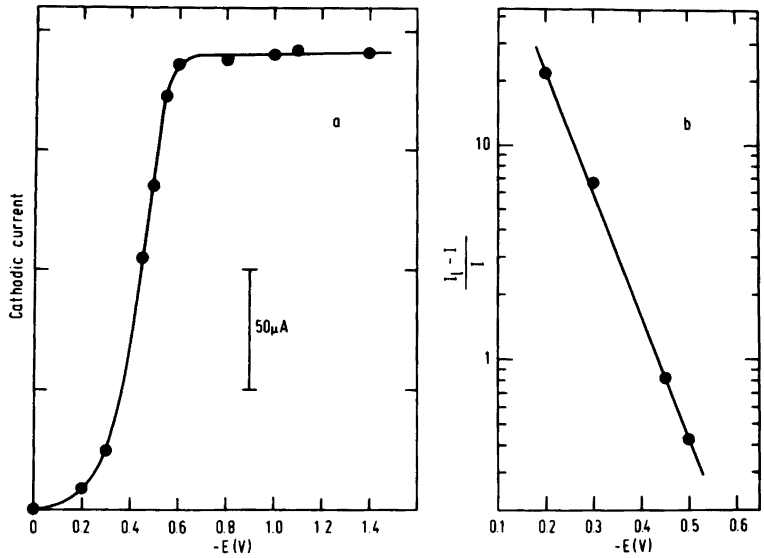

Fig. 11. (a) Current-potential curve constructed from chronoamperometric curves for the reduction of Cl_2 at a plane vitreous carbon electrode in acidic $AlCl_3$–NaCl melt at 162 °C. (b) Semilogarithmic plot of $(I_l - I)/I$ *versus* E for the same wave. Current measured at t=2s. Electrode area, A=0.0535 cm^2.

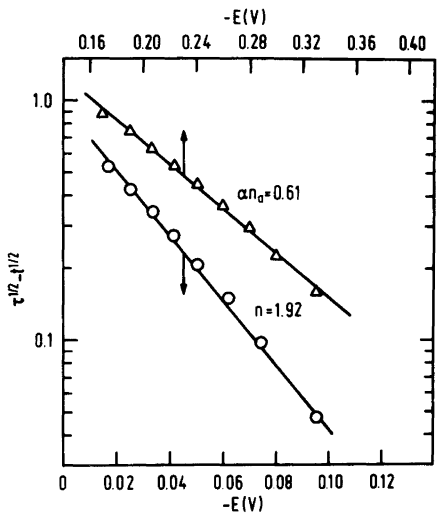

Fig. 12. Analysis of chronopotentiometric curves for the reduction of Cl_2 at a plane vitreous carbon electrode in $AlCl_3$–CsCl melts. △ – 390 °C, τ=1.95 s, acidic melt; ○ – 448 °C, τ=0.743 s, basic melt.

is shown. From the slope of the straight line αn_a is determined to be 0.50 (eqn. (10)).

For the reduction of chlorine in $AlCl_3$–NaCl melts, the αn_a values presented above suggest a one-electron transfer in the rate-determining step with $\alpha \approx 0.5$. This is in fair agreement with results reported for chlorine reduction in $AlCl_3$–NaCl–KCl mixtures.[35,36]

Voltammograms recorded in basic $AlCl_3$–CsCl melts appear to have a different shape relative to those recorded in acidic melts. Curves recorded in an acidic melt were similar to those obtained in $AlCl_3$–NaCl melts. Typical curves for a basic melt are shown in Fig. 7. For acidic melts the shift in peak potentials corresponds to αn_a=0.66. In basic melts the peaks are sharper, and for $v<1$ V s^{-1} E_p is nearly constant. Due to the apparent lack of an overpotential for the cathodic reaction, the curves are so steep that $E_p - E_{p/2} \approx E_p \approx -30$ mV. For a reversible two-electron reduction with soluble products at activity 1 the theoretical value at 262 °C is −21 mV (eqn. (13)). The experimental values of $i_p v^{-1/2}/i\tau^{1/2}$ and $i_p v^{-1/2}/it^{1/2}$ are also somewhat different from the expected results.

The same change in reduction mechanism with respect to melt composition is observed when an analysis of the chronopotentiometric curves is performed. This is illustrated in Fig. 12. The slopes of the curves [eqns. (6) and (7)] yield αn_a=0.61 (acidic melt) and n=1.92 (basic melt). Roughly the same values are obtained from analysis of current–potential curves like that shown in Fig. 7. The different reduction mechanism for chlorine in $AlCl_3$–CsCl melt may be due to the change in acid-base behaviour of the melt and/or if the complex ion Cl_3^- exists (basic melts), it may make the reaction more reversible.

CONCLUDING REMARKS

The diffusion coefficient of chlorine in molten chlorides does not seem to vary markedly with the nature of the salt. In the temperature range 160–890 °C the diffusion coefficient increases from $\sim 2\times10^{-5}$ to $\sim 3\times10^{-4}$ cm^2 s^{-1}.

The chlorine solubilities obtained in the $AlCl_3$–CsCl system indicate a constant solubility in the concentration range $0.425 < X_{AlCl_3} < 0.52$.

An interesting extension of the present work would be to investigate the magnesium chloride–alkali chloride systems where the literature data show a decreasing diffusion coefficient of chlorine with increasing $MgCl_2$ content.[37] These systems are also of interest with respect to the industrial magnesium electrolysis.

Acknowledgements. Experimental assistance of Bente Faaness is gratefully acknowledged. This work has been supported financially by *Norsk Hydro a.s.* and *Norges Teknisk–Naturvitenskapelige Forskningsråd.*

REFERENCES

1. Wærnes, O., Palmisano, F. and Østvold, T. *Acta Chem. Scand. A 37* (1983) 207.
2. Wærnes, O. *Thesis,* Universitetet i Trondheim, Norges tekniske høgskole, Institutt for uorganisk kjemi, Trondheim 1981.
3. Andresen, R. *Thesis,* Universitetet i Trondheim, Norges tekniske høgskole, Institutt for uorganisk kjemi, Trondheim 1976.
4. Delahay, P. *New Instrumental Methods in Electrochemistry,* Interscience, New York 1954.
5. Lorenz, W. *Z. Elektrochem. 59* (1955) 730.
6. Reinmuth, W. H. *Anal. Chem. 33* (1961) 322.
7. Laitinen, H. A. *Anal. Chem. 33* (1961) 1458.

8. Bard, A. J. *Anal. Chem. 33* (1961) 11.
9. Bard, A. J. *Anal. Chem. 35* (1963) 340.
10. Tatwawadi, S. V. and Bard, A. J. *Anal. Chem. 36* (1964) 2.
11. Laitinen, H. A. and Chambers, L. M. *Anal. Chem. 36* (1964) 5.
12. Reinmuth, W. H. *Anal. Chem. 32* (1960) 1514.
13. Paunovic, M. *J. Electroanal. Chem. 14* (1967) 447.
14. Delahay, P. and Berzins, T. *J. Am. Chem. Soc. 75* (1953) 2486.
15. Mamantov, G., Manning, D. L. and Dale, J. M. *J. Electroanal. Chem. 9* (1965) 253.
16. Laitinen, H. A. *Pure Appl. Chem. 15* (1967) 227.
17. Oldham, K. B. and Osteryoung, R. A. *J. Electroanal. Chem. 11* (1966) 397.
18. Berzins, T. and Delahay, P. *J. Am. Chem. Soc. 75* (1953) 555.
19. Nicholson, R. S. and Shain, I. *Anal. Chem. 36* (1964) 706.
20. Matsuda, H. and Ayabe, Y. *Z. Elektrochem. 59* (1955) 494.
21. Delahay, P. *J. Am. Chem. Soc. 75* (1953) 1190.
22. Andresen, R. E., Østvold, T. and Øye, H. A. In Pemsler, J. P., Braunstein, J., Morris, D. R., Nobe, K. and Richards, N. E., Eds., *Proc. Int. Symp. Molten Salts*, The Electrochem. Soc., Princeton, N. J. 1976, p. 111.
23. Carpio, R. A., King, L. A., Ratvik, A. P., Østvold, T. and Øye, H. A. *Light Metals 1981,* 110th AIME Annual Meeting, Chicago 1981, p. 325.
24. Ratvik, A. P. *Private communication,* Universitetet i Trondheim, Norges tekniske høgskole, Institutt for uorganisk kjemi, Trondheim 1982.
25. Van der Kamp, L. K. and van Spronsen, J. W. *Z. Anorg. Allg. Chem. 361* (1968) 328.
26. Øye, H. A. *Private communication.* Universitetet i Trondheim, Norges tekniske høgskole, Institutt for uorganisk kjemi, Trondheim 1981.
27. Stupina, A. M., Bezvoritnii, V. A., Baibakov, D. P., Mukliev, V. I. and Bezukladnikov, A. B. *Tr. Veses. Naucho Issled. Proektn. Inst. Alyumin., Magn. i Elektrod. Prom-sti 101* (1978) 82.
28. Kowalski, M. and Harrington, G. W. *Inorg. Nucl. Chem. Lett. 3* (1967) 121.
29. Mukliev, V. I., Stupina, A. M., Bezvoritnii, V. A., Baibakov, D. P. and Bezukladnikov, A. B. *Fiz. Khim. Elektrokhim. Rasplavl. Tverd. Elektrolitov, Tezisy Dokl. Vses. Konf. Fiz. Khim. Ionnykk Rasplavov Tverd. Elektrolitov, 7th 1* (1979) 48.
30. Vetyukov, M. M., Borisoglebskii, Yu. V. and Hung Bui Van, *Tsvetn. Met. 7* (1981) 45.
31. Boxall, L. G., Jones, H. L. and Osteryoung, R. A. *J. Electrochem. Soc. 120* (1973) 223.
32. Minh, N. Q. and Welch, B. J. *Aust. J. Chem. 28* (1975) 965.
33. Desimoni, E., Paniccia, F. and Zambonin, P. G. *J. Electroanal. Chem. 38* (1972) 373.
34. Desimoni, E., Palmisano, F. and Zambonin, P. G. *J. Electroanal. Chem. 84* (1977) 323.
35. Skundin, A. M., Palanker, V. Sh. and Bagotskii, V. S. *Sov. Electrochem. 2* (1966) 1325.
36. Holleck, G. L. *J. Electrochem. Soc. 119* (1972) 1158.
37. Ukshe, E. A., Leonova, L. S., Yavonova, G. N. and Bukhun, N. G. *Sov. Electrochem. 7* (1971) 373.

Received August 19, 1982.